*Inorg. Chem.* **2007**, *46*, 9895–9905


# A Tetracopper(II)-Tetraradical Cuboidal Core and Its Reactivity as a Functional Model of Phenoxazinone Synthase†

**Chandan Mukherjee,§ Thomas Weyhermüller,§ Eberhard Bothe,§ Eva Rentschler,‡ and Phalguni Chaudhuri*,§**

*Institute for Inorganic and Analytical Chemistry, University of Mainz, D-55128 Mainz, Germany, and Max-Planck-Institute for Bioinorganic Chemistry, Stiftstrasse 34-36, D-45470 Mülheim an der Ruhr, Germany*

Received June 27, 2007

The coordination chemistry of the tridentate ligand *N*-(2-hydroxy-3,5-di-*tert*-butylphenyl)-2-aminobenzylalcohol $H_3L$ has been studied with the copper(II) ion. The ligand is noninnocent in the sense that it is readily oxidized in the presence of air to its *o*-iminobenzosemiquinonato $[L^{\bullet}]^{2-}$ radical form. The crystal structure of the synthesized tetracopper(II)-tetraradical complex $[Cu^{II}_4(L^{\bullet})_4]$ (**1**), has been determined by X-ray crystallography at 100 K. Variable-temperature (2–290 K) magnetic susceptibility measurements of complex **1** containing eight paramagnetic centers establish the spin ground state to be diamagnetic ($S_t = 0$) arising from the antiferromagnetic interactions. Electrochemical measurements (cyclic voltammograms and square wave voltammograms) indicate four one-electron reductions of the ligand prior to the reduction of the metal center. Complex **1** is found to catalyze the aerial oxidation of 2-aminophenol to 2-amino-phenoxazine-3-one, thus modeling the catalytic function of the copper-containing enzyme phenoxazinone synthase. Kinetic measurements together with electron paramagnetic resonance and electronic spectral studies have been used to decipher the complex six-electron oxidative coupling of 2-aminophenol. An "on–off" mechanism of the radicals together with redox participation of the metal center is proposed for the catalytic oxidation processes.

## Introduction

Multicopper oxidases[1] are an important class of oxidases, reducing dioxygen in a four-electron oxidation of the reducing substrate. Multicopper oxidases contain three copper-binding motifs: type 1 (blue), type 2 (normal), and type 3 (binuclear) centers. The most studied and characterized members of this family are laccase, ascorbate oxidase, and ceruloplasmin. Laccase[2] is the simplest blue multicopper oxidase, with one of each type of copper center for a total stoichiometry of four metal ions per protein molecule. The reduction of dioxygen to water presumably occurs in a type 2/type 3 cluster of three copper centers whereas the primary acceptor of electrons from the reducing substrate is a type 1 "blue copper" center, from which the electron is transferred intramolecularly to the $O_2$-reducing cluster. But the detailed mechanism of dioxygen reduction by blue multicopper oxidases is not completely understood.[3]

Phenoxazinone synthase (PHS),[4] a multicopper oxidase, catalyzes the last step in the biosynthesis of the antibiotic actinomycin D by *Streptomyces antibioticus*, namely, the oxidative condensation of two molecules of 3-hydroxy-4-methylanthranilic acid pentapeptide lactone to form

the phenoxazinone chromophore of the most potent antineoplastic agent actinomycin D. The oxidative coupling of the two molecules of substituted 2-aminophenol to produce the phenoxazinone chromophore involves a six-electron oxidation that is thought to take place in a series of three

* To whom correspondence should be addressed. E-mail: Chaudh@mpi-muelheim.mpg.de.

† Dedicated to Karl Wieghardt on the occasion of his 65th birthday.

‡ University of Mainz.

§ Max-Planck-Institute for Bioinorganic Chemistry.

(1) *Multicopper Oxidases*; Messerschmidt, A., Ed.; World Scientific: Singapore,1997.

(2) Solomon, E. I.; Sundaram, U. M.; Machonkin, T. E. *Chem. Rev.* **1996**, *96*, 2563.

(3) Solomon, E. I.; Szilagyi, R. K.; George, S. D.; Basumallick, L. *Chem. Rev.* **2004**, *104*, 419.

(4) (a) Choy, H. A.; Jones, G. H. *Arch. Biochem. Biophys.* **1981**, *211*, 55. (b) Barry, C. E., III; Nayar, P. G.; Begley, T. P. *J. Am. Chem. Soc.* **1988**, *110*, 3333. (c) Barry, C. E., III; Nayar, P. G.; Begley, T. P. *Biochemistry* **1989**, *28*, 6323. (d) Freeman, J. C.; Nayar, P. G.; Begley, T. P.; Willafranca, J. J. *Biochemistry* **1993**, *32*, 4826.

10.1021/ic7012599 CCC: $37.00 
Published on Web 10/16/2007

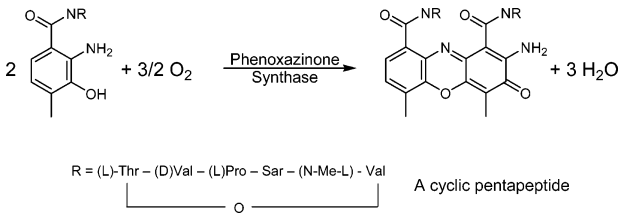


two-electron oxidations, unique among the multicopper oxidases, which usually catalyze one-electron oxidation reactions.

PHS is unique among the multicopper oxidases in that it exists in two oligomeric forms with distinct catalytic activities: low activity dimers and high activity hexamers. Recently, the structure of hexameric PHS[5] has been determined using X-ray diffraction to a resolution limit of 2.30 Å. Each subunit of the hexamer contains five copper atoms as detected earlier spectroscopically.[4c] The structure confirms the presence of all three copper-binding motifs, as usually known for multicopper oxidases: one type 1 (blue), two type 2 (normal), and one binuclear type 3 centers. The location of the fifth copper center, a type 2 copper, at a distance of ~25 Å from the blue copper and the other normal type 2 copper, and the requirement of five copper atoms for maximum activity suggest that the fifth copper atom is not merely advantageously bound but has a structural role, as well. The tetracopper unit of PHS containing one type 1, one type 2, and one type 3 copper centers is shown schematically in Figure 1.

With available physicochemical spectroscopic and crystallographic data as a back-up, the enzyme PHS is "ripe" to encourage us to investigate a bioinspired catalysis aimed at the functional simulation of such enzymes on a molecular level. We have started investigations of radical-containing metal complexes and their oxidative catalytic activities toward different organic substrates in the presence of molecular oxygen as the sole oxidant.[6−9] The aim is twofold: (i) to gain deeper insight into the electronic structure of the metal core and the ligand surrounding of these complexes and, thereby, to better understand such metal radical interactions in natural systems; and (ii) to explore the aerial-oxidation chemistry of well-characterized metal complexes, which is expected to provide the basis for new catalytic oxidation systems for synthetic and industrial processes.

This work stems from our continuing interest in redox-active ligands, based on *N*-phenyl-2-aminophenol,[7,8,10] which can coordinate to a metal not only in their different deprotonated forms but also in their oxidized *o*-iminobenzosemiquinonate radical forms, as depicted in Chart 1. As a natural progression of using radical-generating aminophenol-based ligands and as the alkoxide functionality renders the formation of the $Cu_4O_4$ core, as is evident from the literature,[11] we are prompted to use benzylalcohol as a pendent arm and have synthesized the tridentate ligand $H_3L$, *N*-(2-hydroxy-3,5-di-*tert*-butylphenyl)-2-aminobenzylalcohol and its copper(II) complex **1**. The crystal structure and magnetism of **1** unambiguously show the presence of four copper(II) centers coordinated to four monoradical dianionic forms of the ligand, shown in Chart 1. In this paper, we describe the spectroscopic, electrochemical, and structural characterization of the tetracopper-tetraradical complex **1**, which also exhibits the ability to catalytically generate

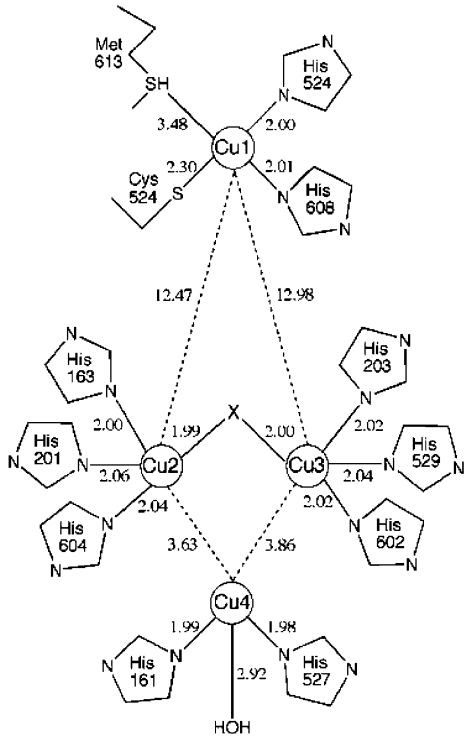


**Figure 1.** Schematic diagram of four conserved copper atoms and their surrounding ligands together with the bonding and nonbonding distances in Å (adapted from ref 5).

(5) Smith, A. W.; Camara-Artigas, A.; Wang, M.; Allen, J. P.; Francisco, W. A. *Biochemistry* **2006**, *45*, 4378.
(6) Chaudhuri, P.; Wieghardt, K.; Weyhermüller, T.; Paine, T. K.; Mukherjee, S.; Mukherjee, C. *Biol. Chem.* **2005**, *386*, 1023.
(7) Mukherjee, C.; Weyhermüller, T.; Bothe, E.; Chaudhuri, P. *C. R. Chim.* **2007**, *10*, 313.
(8) Mukherjee, S.; Weyhermüller, T.; Bothe, E.; Wieghardt, K.; Chaudhuri, P. *Dalton Trans.* **2004**, 3842.
(9) Chaudhuri, P.; Hess, M.; Weyhermüller, T.; Wieghardt, K. *Angew. Chem.* **1999**, 111, 1165. Chaudhuri, P.; Hess, M.; Weyhermüller, T.; Wieghardt, K. *Angew. Chem., Int. Ed.* **1999**, *38*, 1095.
(10) See, for example: (a) Verani, C. N.; Gallert, S.; Bill, E.; Weyhermüller, T.; Wieghardt, K.; Chaudhuri, P. *Chem. Commun.* **1999**, 1747. (b) Chaudhuri, P.; Verani, C. N.; Bill, E.; Bothe, E.; Weyhermüller, T.; Wieghardt, K. *J. Am. Chem. Soc.* **2001**, *123*, 2213. (c) Chun, H.; Verani, C. N.; Chaudhuri, P.; Bothe, E.; Bill, E.; Weyhermüller, T.; Wieghardt, K. *Inorg. Chem.* **2001**, *40*, 4157. (d) Chun, H.; Chaudhuri, P.; Weyhermüller, T.; Wieghardt, K. *Inorg. Chem.* **2002**, *41*, 790. (e) Mukherjee, S.; Weyhermüller, T.; Wieghardt, K.; Chaudhuri, P. *Dalton Trans.* **2003**, 3483. (f) Mukherjee, S.; Rentschler, E.; Weyhermüller, T.; Wieghardt, K.; Chaudhuri, P. *Chem. Commun.* **2003**, 1828. (g) Kokatam, S.; Weyhermüller, T.; Bothe, E.; Chaudhuri, P.; Wieghardt, K. *Inorg. Chem.* **2005**, *44*, 3709. (h) Mukherjee, C.; Weyhermüller, T.; Wieghardt, K.; Chaudhuri, P. *Dalton Trans.* **2006**, 2169.
(11) Selected examples: (a) Thompson, J. S.; Calabrese, J. C. *Inorg. Chem.* **1985**, *24*, 3167. (b) Thompson, J. S.; Calabrese, J. C. *J. Am. Chem. Soc.* **1986**, *108*, 1903. (c) Buchanan, R. M.; Wilson-Blumenberg, C.; Trapp, C.; Larsen, S. K.; Greene, D. L.; Pierpont, C. G. *Inorg. Chem.* **1986**, *25*, 3070. (d) Gojon, E.; Latour, J.-M.; Greaves, S. J.; Povey, D. C.; Ramdas, V.; Smith, G. W. *J. Chem. Soc., Dalton Trans.* **1990**, 2043.

**Chart 1.** Complex **1:** $[Cu^{II}_4(L\bullet)_4]$

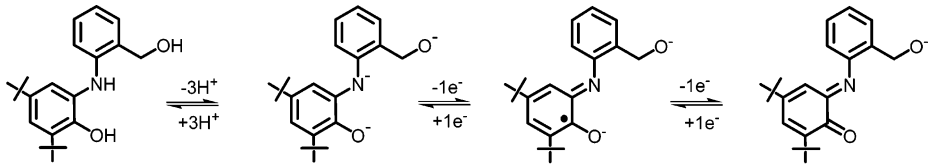


Complex **1:** $[Cu^{II}_4(L^{\bullet})_4]$

**Table 1.** Crystallographic Data and Structure Refinement for Complex **1**·1.5$CH_3CN$·0.5$CH_2Cl_2$

| | |
|---|---|
| empirical formula | $C_{87.5}H_{109.5}Cl_1N_{4.5}O_8Cu_4$ |
| $T$ (K) | 100(2) |
| wavelength (Mo Kα, Å) | 0.71073 |
| cryst syst | monoclinic |
| space group | $P2_1/n$ |
| unit cell dimens | $a = 16.3153(5)$ Å |
| | $b = 29.2224(8)$ Å |
| | $c = 17.7048(5)$ Å |
| | $\alpha = 90^o$ |
| | $\beta = 100.281(5)^o$ |
| | $\gamma = 90^o$ |
| $V$ (Å$^3$), $Z$ | 8305.6(4), 4 |
| density (calc, Mg/m$^3$) | 1.324 |
| abs coeff (mm$^{-1}$) | 1.100 |
| $F$(000) | 3480 |
| cryst size (mm) | 0.37 × 0.33 × 0.22 |
| $\theta$ range for data collect (deg) | 2.94 to 30.98 |
| index range | $-23 \le h \le 23$ |
| | $-32 \le k \le 42$ |
| | $-25 \le l \le 25$ |
| reflns collected | 96 664 |
| independent reflns | 24 851 [$R$(int) = 0.0325] |
| abs correction | Gaussian, face-indexed |
| refinement method | full-matrix least squares on $F^2$ |
| data/restraints/params | 24851/10/1025 |
| goodness-of-fit on $F^2$ | 1.038 |
| final $R$ indices [$I > 2\sigma(I)$] | R1 = 0.0505, wR2 = 0.1210 |
| $R$ indices (all data) | R1 = 0.0717, wR2 = 0.1327 |

phenoxazinone chromophore from 2-aminophenol through aerial oxidation and thus mimics the function of the enzyme PHS.

## Experimental Section

**Materials and Physical Measurements.** Reagent- or analytical-grade materials were obtained from commercial suppliers and used without further purification, except those for electrochemical measurements. Elemental analyses (C, H, N, and metal) were performed by the Microanalytical Laboratory, Mülheim, Germany. Fourier-transform IR spectra of the samples in KBr disks were recorded with a Perkin-Elmer 2000 FT-IR instrument. Electronic absorption spectra in solution were measured with a Perkin-Elmer Lambda 19 spectrophotometer. Magnetic susceptibilities of powdered samples were recorded with a superconducting quantum interference device (SQUID) magnetometer in the temperature range of 2−290 K with an applied field of 1 T. Experimental susceptibility data were corrected for the underlying diamagnetism using Pascal's constants and for the temperature-independent paramagnetism contributions. Mass spectra were recorded with either a Finnigan MAT 8200 (electron ionization, EIMS) or a MAT 95 (electrospray, ESI-MS) instrument. A Bruker DRX 400 instrument was used for NMR spectroscopy. X-band electron paramagnetic resonance (EPR) spectra were recorded with a Bruker ELEXSYS E500 spectrometer equipped with a helium flow cryostat (Oxford Instruments ESR 910). Cyclic voltammograms (CV) were recorded using a conventional three-electrode arrangement, consisting of a glassy-carbon working electrode (of 2 mm diameter), an $Ag/Ag^+$ (0.01 M $AgNO_3$) reference electrode, and a Pt-wire counter electrode. Small amounts of ferrocene were added as an internal standard after completion of an experiment, and potentials are referenced versus the ferrocenium/ferrocene ($Fc^+$/Fc) couple. Potential control was achieved using an EG&G potentiostat/galvanostat (model 273A) with M270 software, and solutions of the complexes in $CH_2Cl_2$ containing 0.2 M $[(n\text{-}Bu)_4N]PF_6$ as supporting electrolyte were employed throughout.

Controlled-potential electrolysis at an appropriate fixed potential was performed at −25 °C in a jacketed quartz cell with the same type of reference electrode, a Pt-mesh working electrode, and a Pt-brush counter electrode. The cell (optical path length 0.5 cm) was mounted directly in a spectrophotometer (Hewlett-Packard HP 8453), allowing us to record UV−vis spectra in situ during electrolysis. After the completion of electrolysis, samples of the electrolyzed solutions were taken and rapidly frozen by liquid nitrogen for electron spin resonance analysis.

**Preparation of the Ligand $H_3L$.** To a solution of 3,5-di-*tert*-butylcatechol (2.25 g; 10 mmol) and triethylamine (0.2 mL) in *n*-hexane (50 mL) was added solid 2-aminobenzylalcohol (1.25 g; 10 mmol). The resulting solution was stirred in air overnight, after which time a white (brownish) solid was collected by filtration, washed with *n*-hexane, and air-dried. The yield was 1.9 g (58%) based on the starting catechol. Mp: 128−129 °C. EI-MS: *m*/*z* 327 (100%) $[M^+]$, 309 (21%) $[M - 18]^+$, 252 (87%) $[M - 18 - C_4H_8]^+$. IR (KBr, cm$^{-1}$): 3515, 3385, 2962−2986, 1603, 1584, 1504, 1480, 1460, 1426, 1225, 1003, 981, 750. $^1$H NMR ($CD_2Cl_2$): $\delta$ = 1.26 (s, 9 $^t$Bu−H), 1.42 (s, 9 $^t$Bu−H), 4.82 (s, $CH_2$−H), 6.48−7.21 (6H, aromatic). Anal. Calcd for $C_{21}H_{29}NO_2$: C, 77.02; H, 8.93; N, 4.28. Found: C, 76.9; H, 8.9; N, 4.3.

**Preparation of $[Cu^{II}_4(L^{\bullet})_4]$ (1).** To a solution of the ligand, $H_3L$ (0.655 g; 2 mmol), in acetonitrile (30 mL) was added solid copper(II) acetate (0.4 g; 2 mmol). Upon the addition of 0.2 mL of $NEt_3$ in the presence of air, the color of the solution changed to green. After stirring of the solution for 24 h, a dark green microcrystalline product of **1** was collected by filtration. Yield: 0.55 g (∼70%). Single crystals suitable for X-ray diffraction were grown from a $CH_2Cl_2/CH_3CN$ solvent mixture (1:1). Anal. Calcd for $C_{21}H_{26}NO_2Cu$: C, 65.01; H, 6.76; N, 3.61; Cu, 16.38. Found: C, 65.8; H, 6.6; N, 3.6; Cu, 15.6. ESI (positive)-MS in $CH_2Cl_2$: *m*/*z* 1550 (90%) $[M]^+$, 1227 (26%) $[L_3Cu_4]^+$, 838 (100%) $[L_2Cu_3]^+$, 713 (42%) $[CuL_2]^+$. IR(KBr, cm$^{-1}$): 2953−2870, 1474, 1460, 1435, 1416, 1257, 1025, 751.

**Procedure for the Oxidation of 2-Aminophenol and Determination of the Concentration of the Phenoxazinone Chromophore.** A solution of 2.5 × 10$^{-4}$ M of **1** and 2.5 × 10$^{-2}$ M

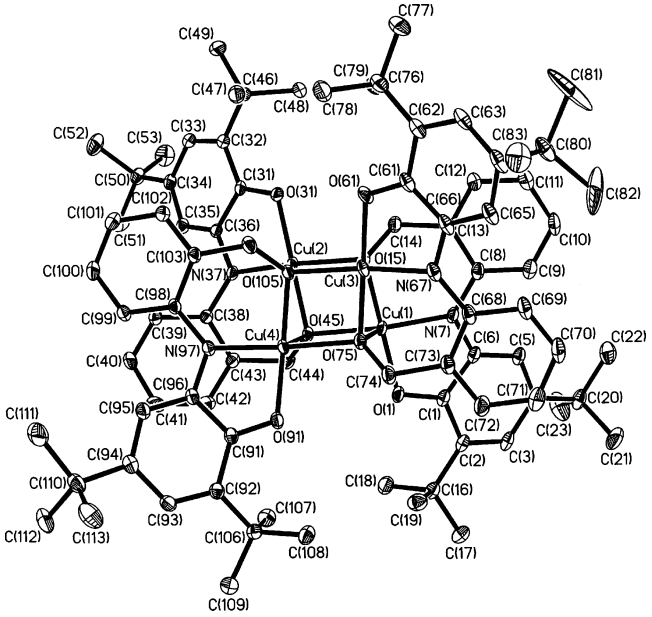


**Figure 2.** ORTEP diagram of the neutral molecule **1**, with 50% probability of the ellipsoids.

2-aminophenol in 20 mL of either methanol or a solvent mixture (4:1) of $CH_2Cl_2/CH_3OH$ was made and stirred in air for the oxidation. The solution was diluted as required for acquisition of the UV−vis spectra, and the concentration of the phenoxazinone chromophore was calculated on the basis of its molar extinction coefficient ($\epsilon_{435} = 24 \times 10^3\ M^{-1}\ cm^{-1}$) at 435 nm.

**Kinetic Experiments.** Reaction kinetics were performed by observing the change in absorbance at 435 nm, which is characteristic of 2-aminophenoxazin-3-one in methanol. In a typical reaction, the catalyst, complex **1**, was dissolved in methanol and the substrate 2-aminophenol was added, and the resulting solution was stirred in the presence of air; the resulting spectral change as a function of time was measured. For the calculation of rate constants, the initial rate method was used and the velocity of the reaction was obtained from the slope of the tangent to the absorbance vs time curve.

The kinetics of the oxidative reaction at a constant catalyst concentration ([complex **1**] $= 2.5 \times 10^{-5}$ M in methanol) were investigated with variation of the substrate concentration ($2.5-25$) $\times 10^{-3}$ M. The difference in absorbance $\Delta A$ at 435 nm was plotted against time to obtain the rate constant for that particular substrate concentration. From variation of the rate constants as a function of substrate concentration, the rate of the reaction with respect to substrate was found. Similar procedures with varying catalyst concentrations, keeping a constant substrate concentration ($6 \times 10^{-3}$ M), yielded different rate constants, thus leading to the result for the order of the reaction with respect to the catalyst.

**X-ray Crystallographic Data Collection and Refinement of the Structure.** A single crystal of **1** was coated with perfluoropolyether, picked up with glass fibers, and mounted on a Nonius Kappa-CCD diffractometer equipped with a cryogenic nitrogen cold stream operating at 100(2) K. Graphite-monochromated Mo K$\alpha$ radiation ($\lambda = 0.71073$ Å) was used. Intensity data were corrected for Lorentz and polarization effects. The intensity data set of **1** was corrected for absorption with the use of the Gaussian, face-indexed program. The Siemens *SHELXTL* software package (G. M. Sheldrick, Universität Göttingen) was used for solution, refinement, and artwork of the structure, and neutral atom scattering factors of the program were used. The structure was solved and refined by direct methods and difference-Fourier techniques. Non-hydrogen atoms were refined anisotropically, and hydrogen atoms were placed at calculated positions and refined as riding atoms with isotropic displacement parameters. Split atom models were used to account for disorder of the solvent molecules. Details of data collection and structure refinements are summarized in Table 1.

**Table 2.** Selected Bond Lengths (Å) and Angles (deg) for **1**

| | | | |
|---|---|---|---|
| Cu(1)−O(1) | 1.9076(15) | Cu(1)···Cu(2) | 2.956(1) |
| Cu(1)−O(15) | 1.9388(14) | Cu(1)···Cu(3) | 3.089(3) |
| Cu(1)−N(7) | 1.9579(18) | Cu(1)···Cu(4) | 3.332(3) |
| Cu(1)−O(45) | 1.9884(14) | Cu(2)···Cu(3) | 3.324(3) |
| Cu(1)−O(75) | 2.3137(15) | Cu(2)···Cu(4) | 3.119(3) |
| Cu(2)−O(31) | 1.9295(14) | Cu(3)···Cu(4) | 2.954(4) |
| Cu(2)−N(37) | 1.9441(17) | | |
| Cu(2)−O(45) | 1.9461(14) | | |
| Cu(2)−O(15) | 1.9904(15) | | |
| Cu(2)−O(105) | 2.2836(14) | | |
| Cu(3)−O(61) | 1.9137(15) | | |
| Cu(3)−O(75) | 1.9277(15) | | |
| Cu(3)−N(67) | 1.9562(18) | | |
| Cu(3)−O(105) | 1.9872(14) | | |
| Cu(3)−O(15) | 2.3147(14) | | |
| Cu(4)−O(91) | 1.9211(15) | | |
| Cu(4)−N(97) | 1.9448(18) | | |
| Cu(4)−O(105) | 1.9520(14) | | |
| Cu(4)−O(75) | 1.9934(15) | | |
| Cu(4)−O(45) | 2.2891(14) | | |

| | | | |
|---|---|---|---|
| O(1)−Cu(1)−O(15) | 177.99(6) | N(67)−Cu(3)−O(105) | 166.11(7) |
| O(1)−Cu(1)−N(7) | 85.19(7) | O(61)−Cu(3)−O(15) | 97.16(6) |
| O(15)−Cu(1)−N(7) | 94.49(7) | O(75)−Cu(3)−O(15) | 85.36(6) |
| O(1)−Cu(1)−O(45) | 98.00(6) | N(67)−Cu(3)−O(15) | 114.97(6) |
| O(15)−Cu(1)−O(45) | 81.84(6) | O(105)−Cu(3)−O(15) | 78.24(5) |
| N(7)−Cu(1)−O(45) | 165.88(7) | O(61)−Cu(3)−Cu(4) | 137.58(5) |
| O(1)−Cu(1)−O(75) | 96.80(6) | O(75)−Cu(3)−Cu(4) | 41.95(4) |
| O(15)−Cu(1)−O(75) | 85.14(6) | N(67)−Cu(3)−Cu(4) | 132.01(5) |
| N(7)−Cu(1)−O(75) | 115.25(7) | O(105)−Cu(3)−Cu(4) | 40.96(4) |
| O(45)−Cu(1)−O(75) | 78.17(5) | O(15)−Cu(3)−Cu(4) | 85.44(4) |
| O(1)−Cu(1)−Cu(2) | 137.62(5) | O(91)−Cu(4)−N(97) | 84.32(7) |
| O(15)−Cu(1)−Cu(2) | 41.87(4) | O(91)−Cu(4)−O(105) | 175.78(6) |
| N(7)−Cu(1)−Cu(2) | 132.09(5) | N(97)−Cu(4)−O(105) | 93.73(7) |
| O(45)−Cu(1)−Cu(2) | 40.76(4) | O(91)−Cu(4)−O(75) | 99.20(6) |
| O(75)−Cu(1)−Cu(2) | 85.11(4) | N(97)−Cu(4)−O(75) | 159.58(7) |
| O(31)−Cu(2)−N(37) | 84.21(7) | O(105)−Cu(4)−O(75) | 81.34(6) |
| O(31)−Cu(2)−O(45) | 175.68(6) | O(91)−Cu(4)−O(45) | 100.81(6) |
| N(37)−Cu(2)−O(45) | 93.52(6) | N(97)−Cu(4)−O(45) | 120.65(6) |
| O(31)−Cu(2)−O(15) | 99.40(6) | O(105)−Cu(4)−O(45) | 83.41(5) |
| N(37)−Cu(2)−O(15) | 161.48(7) | O(75)−Cu(4)−O(45) | 78.67(5) |
| O(45)−Cu(2)−O(15) | 81.61(6) | O(91)−Cu(4)−Cu(3) | 137.83(5) |
| O(31)−Cu(2)−O(105) | 100.63(6) | N(97)−Cu(4)−Cu(3) | 128.95(5) |
| N(37)−Cu(2)−O(105) | 118.46(6) | O(105)−Cu(4)−Cu(3) | 41.86(4) |
| O(45)−Cu(2)−O(105) | 83.68(5) | O(75)−Cu(4)−Cu(3) | 40.28(4) |
| O(15)−Cu(2)−O(105) | 78.94(5) | O(45)−Cu(4)−Cu(3) | 84.40(4) |
| O(31)−Cu(2)−Cu(1) | 138.32(5) | C(1)−O(1)−Cu(1) | 111.62(14) |
| N(37)−Cu(2)−Cu(1) | 129.59(5) | C(31)−O(31)−Cu(2) | 111.66(12) |
| O(45)−Cu(2)−Cu(1) | 41.84(4) | C(61)−O(61)−Cu(3) | 111.82(14) |
| O(15)−Cu(2)−Cu(1) | 40.55(4) | C(91)−O(91)−Cu(4) | 111.68(13) |
| O(105)−Cu(2)−Cu(1) | 84.66(4) | | |
| O(61)−Cu(3)−O(75) | 177.44(6) | | |
| O(61)−Cu(3)−N(67) | 85.06(7) | | |
| O(75)−Cu(3)−N(67) | 94.32(7) | | |
| O(61)−Cu(3)−O(105) | 97.92(6) | | |
| O(75)−Cu(3)−O(105) | 82.10(6) | | |

## Results and Discussion

**Molecular Structure of 1.** The crystal structure of **1** is shown in Figure 2, with selected bond lengths and angles provided in Table 2.

The neutral molecule **1** contains four O,N,O-coordinated alkoxo *o*-iminobenzosemiquinonato radical dianions, $[L^{\bullet}]^{2-}$, as shown in Chart 1. The metrical details of each of the four

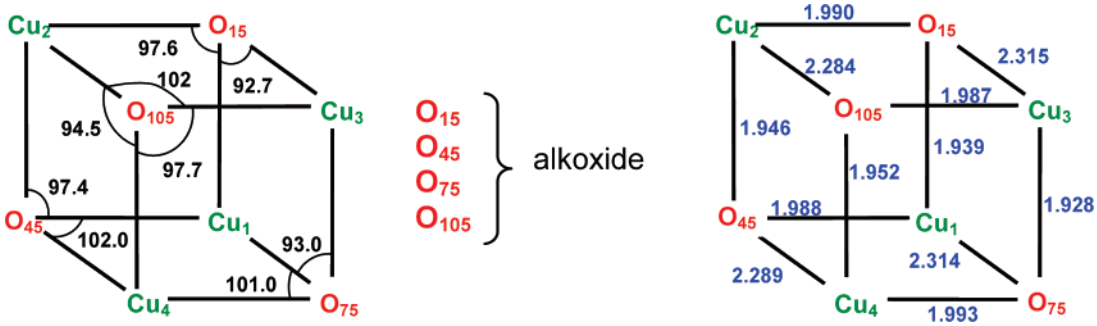


**Figure 3.** Schematic representations of selected Cu−O−Cu bond angles and Cu−O bond lengths within the $Cu_4O_4$ cube. The remaining angles are Cu(2)−O(15)−Cu(3) = 100.8°, Cu(2)−O(45)−Cu(4) = 94.5°, and Cu(3)−O(75)−Cu(4) = 97.8°.

ligands can best be represented by two classical resonance structures of A and B.

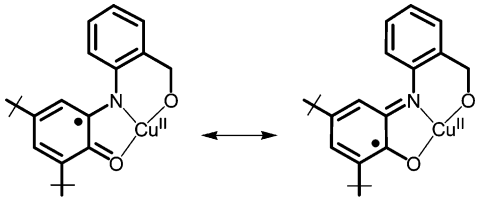


The imino C═N bonds at 1.358 ± 0.005 Å are significantly shorter than the $C_{benzyl}$−N bonds at 1.398 ± 0.005 Å. The average $C_{phenyl(t)}$−O bond distance at 1.298 ± 0.004 Å (where phenyl(*t*) represents the *tert*-butyl-containing phenyl ring) is also remarkably shorter than the 1.35−1.37 Å expected for a coordinated catecholate; it is in the range of those reported for transition-metal *o*-benzosemiquinonato-(1−) complexes.[10,11] The six ring C−C distances in the *o*-iminosemiquinonato part, i.e., the $C_6$ ring with the *tert*-butyl groups, are not equidistant, whereas the six C−C distances of the N(benzyl alcohol) part are within experimental error; the same at 1.40 ± 0.02 Å. In the *o*-iminobenzosemiquinonato part, two alternating relatively short C═C distances are observed at 1.376 ± 0.008 Å and four longer C−C bonds are observed at 1.435 ± 0.015 Å in the four six-membered rings. The difference of 0.059 Å between these two average values is larger than the experimental error of ±0.015 Å. Therefore, the oxidation level of the ligand $[L^{\bullet}]^{2-}$ is considered to be correctly represented by the resonance structures A and B. Summarily, all the phenyl rings with the *tert*-butyl substituents are in the radical iminosemiquinone form with the quinoid-type distortion.

The solid-state structure of **1** is based on a $Cu_4O_4$ cubane-type unit and consists of two interpenetrating pseudotetrahedra, one of four copper atoms and one of four $\mu_3$-oxygen atoms originating from bridging alkoxide groups. Each copper is pentacoordinated with one imine N, one phenolate, and three $\mu_3$-alkoxo O atoms. The geometry around each copper ion with $CuNO_4$ environments is best described as that of distorted square pyramidal with $\tau$ values varying between 0.18 and 0.26, where $\tau$ is an index of trigonality for five-coordinate environments. $\tau$ is zero for a perfect square pyramid, while it becomes unity for a trigonal-bipyramidal geometry.[12] The axial Cu−O (alkoxide) bond lengths are as expected, comparatively long with an average length of 2.300 Å. The basal Cu−O (alkoxide) bond lengths vary between 1.928(2) and 1.993(2) Å, whereas the basal Cu−O (semiquinone) bond distances lie in a small range of 1.908(2)−1.930(1) Å. All Cu−N bonds are in the basal plane with an average distance of 1.951 Å and have been observed in other cubane complexes containing Cu(II) and coordinated alkoxides.[13] Complex **1** thus must contain four copper(II) centers and all four ligands in the oxidized iminobenzosemiquinone forms also supported by the electrochemistry, magnetic, and spectroscopic measurements. The Cu−$O_{alk}$ bond lengths and the bond angles Cu−$O_{alk}$−Cu, where $O_{alk}$ stands for the alkoxo oxygen atoms, are shown schematically in Figure 3.

All benzyl rings of the ligands are planar and retain their aromaticity after complexation. The Cu−O−Cu angles vary between 92.73(6)° and 102.08(6)°. The Cu···Cu distances on different cubic faces are also different, the shortest being Cu(1)···Cu(2) = 2.956(1) Å and the longest being Cu(1)···Cu(4) = 3.332(3) Å (Table 2).

**Magnetic Susceptibility Measurements.** Variable-temperature magnetic susceptibility measurements were carried out in the temperature range of 2−290 K in an applied magnetic field of 1 T on a polycrystalline sample of **1** with a SQUID magnetometer. The temperature dependence of the susceptibility of complex **1** containing eight paramagnetic centers of $S_{Cu} = S_R = {}^1/_2$ is displayed in Figure 4 in the form $\chi_M T$ vs $T$. The $\chi_M T$ vs $T$ curve for **1** exhibits antiferromagnetic coupling with a decrease of $\chi_M T$ from a high-temperature (290 K) value of 3.102 $cm^3$ K $mol^{-1}$ ($\mu_{eff}$

(12) (a) Muetterties, E. L.; Guggenberger, L. J. *J. Am. Chem. Soc.* **1974**, *96*, 1748. (b) Addison, A. W.; Nageswara Rao, T.; Reedijk, J.; van Rijn, J.; Verschoor, G. C. *J. Chem. Soc., Dalton Trans.* **1984**, 1349.

(13) Representative examples: (a) Merz, L.; Haase, W. *J. Chem. Soc., Dalton Trans.* **1978**, 1594. (b) Mergehenn, R.; Merz, L.; Haase, W. *J. Chem. Soc., Dalton Trans.* **1980**, 1703. (c) Laurent, J.-P.; Bonnet, J.-J.; Nepveu, F.; Astheimer, H.; Walz, L.; Haase, W. *J. Chem. Soc., Dalton Trans.* **1982**, 2433. (d) Dedert, P. L.; Sorrell, T.; Marks, T. J.; Ibers, J. A. *Inorg. Chem.* **1982**, *21*, 3506. (e) Walz, L.; Paulus, H.; Haase, W.; Langhof, H.; Nepveu, F. *J. Chem. Soc., Dalton Trans.* **1983**, 657. (f) Sletten, J.; Sorensen, A.; Julve, M.; Journaux, Y. *Inorg. Chem.* **1990**, *29*, 5054. (g) Mukherjee, A.; Raghunathan, R.; Saha, M. K.; Nethaji, M.; Ramasesha, S.; Chakravarty, A. R. *Chem.—Eur. J.* **2005**, *11*, 3087. (h) Tan, X. S.; Fujii, Y.; Nukada, R.; Mikuriya, M.; Nakano, Y. *J. Chem. Soc., Dalton Trans.* **1999**, 2415. (i) Xie, Y.; Jian, H.; Chan, A. S.-C.; Liu, Q.; Xu, X.; Du, C.; Zhu, Y. *Inorg. Chim. Acta* **2002**, *333*, 138. (j) Nihei, M.; Hoshino, N.; Ito, T.; Oshio, H. *Polyhedron* **2003**, *22*, 2359.

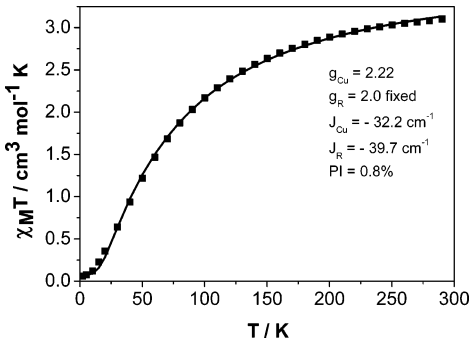


**Figure 4.** Plot of $\chi_M T$ vs $T$ for complex **1**. The solid line represents the best fit of the experimental data using the coupling model (A) shown in Scheme 1.

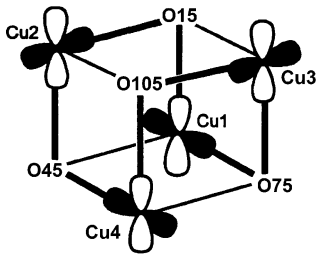


**Figure 5.** Arrangement of the magnetic orbitals within the tetranuclear cuboidal Cu(II) centers in complex **1**.

$= 4.98\ \mu_B$) to a value of 0.059 cm$^3$ K mol$^{-1}$ ($\mu_{eff} = 0.68\ \mu_B$) at 2 K, indicating that the eight paramagnetic centers are coupled together to yield an $S_t = 0$ ground state.

To simulate the experimental magnetic data of complex **1** using the irreducible tensor operator approach,[14] the Heisenberg spin-exchange Hamiltonian in the form

$$\hat{H} = -2 \sum_{i<j} J_{ij}\, \hat{S}_i \cdot \hat{S}_j$$

was considered in which $J_{ij}$ is the exchange integral between the magnetic centers $i$ and $j$. Different models with "one $J$" (i.e., isolated pair of equal Cu(II) dimers), "two $J$" (highest possible symmetry within the $Cu_4O_4$ core $S_4$), and "three $J$" (subgroups of $T_d$ which retain a two-fold axis) have been used in the literature for the analysis of magnetic data of $Cu_4O_4$ cubane-type complexes.[13,15] For example, the magnetic susceptibility of $[Cu(Deae)Cl]_4$ where Deae is 2-diethylaminoethanolato was simulated with the $C_{2v}$ tetramer model.[15d] As for complex **1**, the Cu−radical (Cu−$O_{phenyl}$) bond lengths lying in a small range of 1.91−1.93 Å and the bond angle of Cu−$O_{ph}$−$C_R$ ($C_R$ = radical containing C center) at 111.7° can be considered to be invariable, and the four radical−copper(II) interactions as depicted in Scheme 1 are taken to be equal.

To avoid overparametrization and to use the simplest model possible for complex **1**, we fitted the experimental data by applying a single coupling constant $J_{Cu}$ for the

**Scheme 1.** Exchange Coupling Model[a]

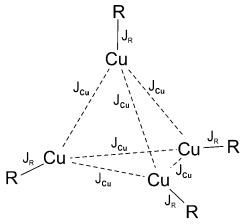


$J_{Cu}$ = interactions between the copper centers
$J_R$ = interactions between the copper and radical centers

[a] Key: $J_{Cu}$ = interactions between the copper centers and $J_R$ = interactions between the copper and radical centers.

intracopper interactions (Scheme 1) and an interaction $J_R$ for the Cu(II)−radical interactions. A good fit is obtained with the parameters $J_{Cu} = -32.2$ cm$^{-1}$, $J_R = -39.7$ cm$^{-1}$, $g_{Cu} = 2.22$, $g_R = 2.0$ (fixed), and Paramagnetic Impurity (PI) = 0.8% and is shown in Figure 4 as the solid line. The copper(II)−radical interactions reported in the literature vary widely from moderate ferromagnetic to strong antiferromagnetic, depending on the mixing of metal d orbitals ($e_g$ parentage) with concomitant removal of a substantial portion of metal−ligand antibonding character. Such comparable antiferromagnetic interactions for the Cu(II)···Cu(II) and the Cu(II)−radical interactions, although stronger, have also been observed earlier.[9,15] Naturally, we prefer the simulation with the these minimum parameters. The model of an isolated pair of equal dimers appears reasonable for **1** in view of the large interdimer Cu−alkoxide axial distances at ∼2.30 Å, which should render any out-of-plane interactions very weak. Moreover, it can be concluded that the intracopper(II) exchange interactions transmitted through the $\mu_3$-alkoxo bridges are negligible in the Cu−$O_{alk}$−Cu bond angle range of 92.73−97.77°, that is, in accord with the results reported earlier.[13,15]

The moderate strength of the antiferromagnetic interactions can be rationalized by considering the orientation of $(d_{x^2-y^2})^1$, the magnetic orbital, as the coordination geometry about each copper is that of square pyramidal. The arrangement of the magnetic orbitals within the tetranuclear cuboidal copper(II) centers is shown in Figure 5; the $d_{x^2-y^2}$ orbitals of the pairs Cu(1)/Cu(4) and Cu(2)/Cu(3) are parallel to each other, whereas for the pairs Cu(1)/Cu(3) and Cu(2)/Cu(4), the orbitals are arranged perpendicularly. It appears that both of the alkoxide−oxygen bridging ligands of the same pairs are axial to one metal atom and equatorial to the other, yielding negligible overlap of the orbitals, and hence, very weak or no antiferromagnetic interactions result. On the other hand, the interpair interaction implies two different types of bridges including one of the axial−equatorial type as above but also one of the equatorial−equatorial type. The latter equatorial−equatorial combination produces a significant overlap on one bridging oxygen, thus providing a pathway albeit moderate to the antiferromagnetic interaction, as observed for $J_{Cu}$. Contrary to the expectation of the ferromagnetic interaction between the $(d_{x^2-y^2})^1$ magnetic orbital at the copper ions and the $\pi$ orbital of the radicals, which are orthogonal relative to each other, the Cu−radical interactions $J_R$ are evaluated to be antiferromagnetic, and

(14) Gatteschi, D.; Pardi, L. *Gazz. Chim. Ital.* **1993**, *123*, 231.
(15) (a) Merz, L.; Haase, W. *J. Chem. Soc., Dalton Trans.* **1980**, 875. (b) Fallon, G. D.; Moubaraki, B.; Murray, K. S.; van den Bergen, A. M.; West, B. O. *Polyhedron* **1993**, *12*, 1989. (c) Wang, S.; Zheng, J.-C.; Hall, J. R.; Thompson, L. K. *Polyhedron* **1994**, *13*, 1039. (d) Hall, J. W.; Estes, W. E.; Estes, E. D.; Scaringe, R. P.; Hatfield, W. E. *Inorg. Chem.* **1977**, *16*, 1572.

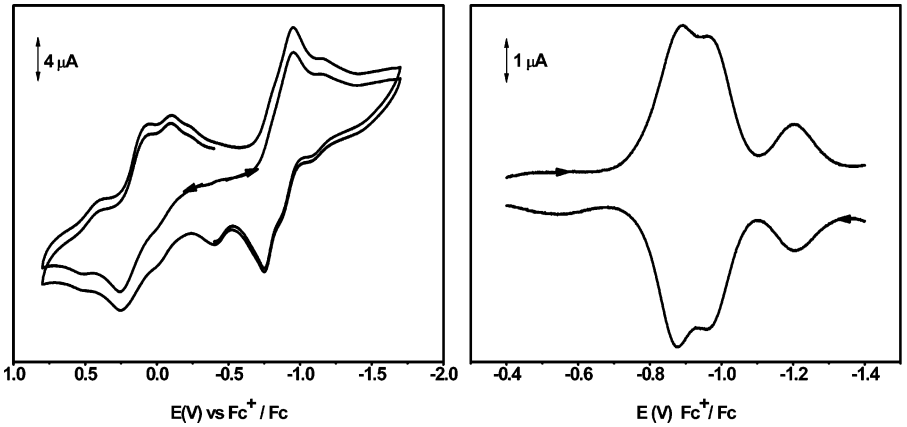


**Figure 6.** CVs and SQWs of complex **1** in $CH_2Cl_2$ at ambient temperature.

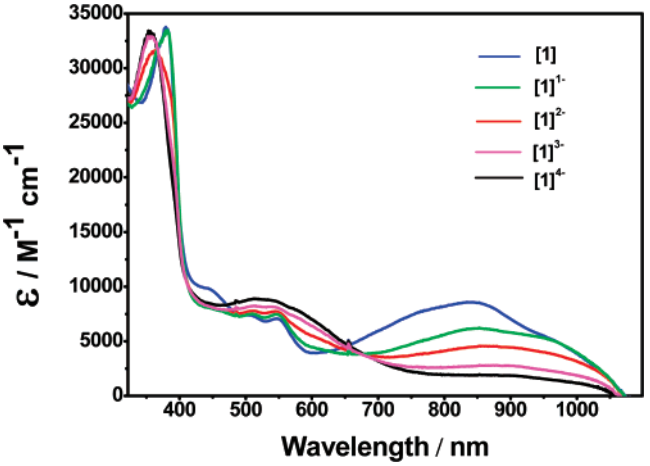


**Figure 7.** Electronic spectra of $[\mathbf{1}]^{1}$, $[\mathbf{1}]^{-}$, $[\mathbf{1}]^{2-}$, $[\mathbf{1}]^{3-}$, and $[\mathbf{1}]^{4-}$ in $CH_2Cl_2$ at −25 °C.

that warrants some rationale. Structural data clearly show that the angle at the phenoxide oxygens, O(1), O(61), O(31), and O(91), is not 90° but is more obtuse at 111.7°, thus destroying the orthogonality between the orbitals of copper and radical oxygens; this leads to a weak but substantial overlap of the said orbitals resulting in the moderate antiferromagnetic interactions.

**Electrochemistry and Spectroelectrochemistry.** CVs and square wave voltammograms (SQWs) of complex **1** have been measured at ambient temperatures in $CH_2Cl_2$ solutions containing 0.2 M $[(n\text{-}Bu)_4N]PF_6$ as the supporting electrolyte. Ferrocene was used as an internal standard, and potentials are referenced versus the ferrocenium/ferrocene ($Fc^+$/Fc) couple. Figure 6 shows CVs in the potential range of +1.4 to −1.8 V (with scans starting in either anodic or cathodic direction) and anodic and cathodic SQWs in the reductive range.

It is seen that the CVs of complex **1** are difficult to analyze because several oxidation and reduction peaks occur in close vicinity. However, symmetric reoxidation waves following the reductions are discernible, and similarly, re-reduction waves after the oxidations, which indicate the largely reversible nature of the underlying redox processes. The peak separations are higher (about 0.2 V) than that for diffusion-controlled electron exchange (0.06 V) and decrease with decreasing scan rate, indicating that the heterogeneous electron transfer is slow.

The individual redox processes can be distinguished better from SQWs. Figure 6 shows that oxidative and reductive scans in the negative (reducing) potential range look identical, which confirms the reversibility of the reductions on the time scale of the voltammetric experiments (the behavior in the oxidation range is more complex and will not be discussed here). It is seen that two reduction peaks at −0.83 and −0.96 V are followed by a third reduction at −1.20 V with lower peak current.

A coulometric experiment (at −25 °C) at a potential immediately "behind" the twin peaks (at −1.1 V) showed that four electrons/molecule are transferred in the reductions represented by the double peak. Figure 7 shows the spectral changes recorded during the stepwise coulometric four-electron reduction of complex **1**. Table 3 summarizes the results. The UV−vis/NIR spectrum of complex **1** shows absorption bands at 380, 550, and 507 nm, with absorption coefficients $\epsilon$ (in $M^{-1}$ $cm^{-1}$) of 33 600, 7065, and 7500, respectively. All these bands may be tentatively assigned to ligand-to-metal charge-transfer bands. The broad band centered around 840 nm is ascribed to ligand-to-ligand charge transfer.[10]

From Figure 7, it is seen that the spectral changes for all four reductions are quite similar. This provides evidence that the reductions are all of the same type. Most noticeable is the successive absorption decrease of the band at around 840 nm, which points to ligand-centered reductions to yield amidophenolate moieties (Chart 1), an assumption which is strongly supported by the results of the EPR measurements (vide infra). During four one-electron reductions, the broad band at around 840 nm shifts to longer wavelengths and decreases in intensity. The final absorption coefficient after four-electron reductions is 1950 $M^{-1}$ $cm^{-1}$ and most probably arising due to the d−d transition of the tetracopper(II) core devoid of any iminosemiquinone radical.

After the first and third one-electron reduction, samples were taken for EPR analysis. Unfortunately, the reductions are not fully reversible on the prolonged time scale required for electrolysis (95 min): In an attempt to reoxidize the reduced form electrochemically, we could get back only two electrons, which indicates decay reactions of the reduced

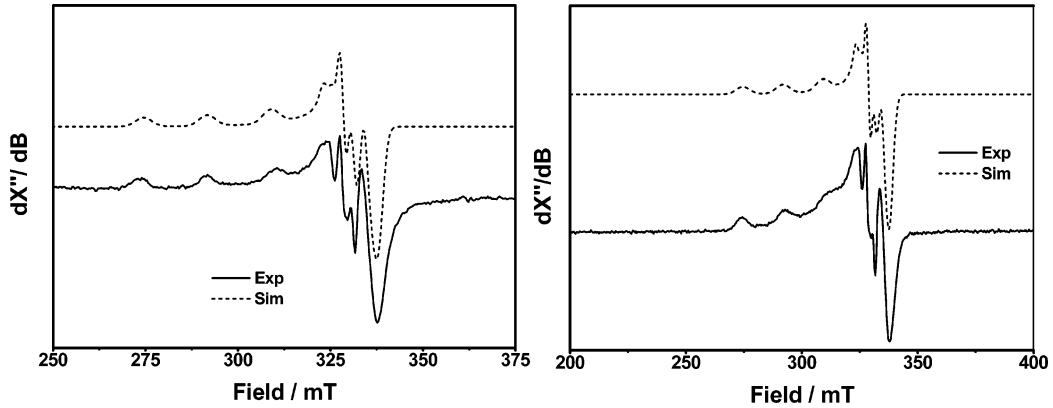


**Figure 8.** X-band EPR spectra of $[\mathbf{1}]^{3-}$ (left) and $[\mathbf{1}]^{-}$ (right), measured at 30 K.

**Table 3.** Electronic Spectral Data Together with the Corresponding Simulated EPR Data of Complex **1** and Its Electrochemically Generated Reduced Species

| complex | $\lambda$, nm ($\epsilon$, $M^{-1}$ $cm^{-1}$) | sim EPR |
|---|---|---|
| [**1**] | 845(8600), 550(7065), 507(7500), 447(9830), 380(33600) | inactive |
| $[\mathbf{1}]^{-}$ | 952(5430), 840(6140), 546(7475), 507(7600), 380(33300) | $g_i = 2.06, 2.033, 2.245$, $A_i = (20, 1, 180) \times 10^{-4}$ $cm^{-1}$ |
| $[\mathbf{1}]^{2-}$ | 860(4500), 544(7800), 507(7800), 362(31600) | inactive |
| $[\mathbf{1}]^{3-}$ | 875(2764), 541(8190), 511(8294), 355(33000) | $g_i = 2.0275, 2.0575, 2.245$, $A_i = (10, 20, 180) \times 10^{-4}$ $cm^{-1}$ |
| $[\mathbf{1}]^{4-}$ | 875(1950), 523(8900), 355(33000) | inactive |

complex during the coulometry. Since the decay is expected to be of major importance in the later stage of electrolysis (when no EPR samples are taken anymore) and since decay reactions yield usually EPR-silent products, we nevertheless consider the results of the EPR measurements as firm evidence for the ligand-centered nature of the first four reduction steps. The further reduction seen in the SQW at more negative potentials (−1.2 V) must then be metal-centered to yield copper(I) ions.

**EPR Spectra of the Electroreduced Species.** The X-band EPR spectra of one-electron and three-electron reduced species,$[\mathbf{1}]^{-}$ and $[\mathbf{1}]^{3-}$, respectively, of complex **1** in $CH_2Cl_2$ at 30 K are depicted in Figure 8 together with their simulations.

The rhombic signals $g_1 = 2.06$, $g_2 = 2.03$, and $g_3 = 2.245$, for example, reveal a spin system $S_t = {}^1/_2$ localized on copper(II), resulting from the electrochemical reductions of the radicals and not of the metal centers. Of complex **1**, the two-electron and the four-electron reduced species, $[\mathbf{1}]^{2-}$ and$[\mathbf{1}]^{4-}$, respectively, are EPR inactive. The small amount of mononuclear impurity (PI $\approx$ 0.8%) present in the sample, as observed in the SQUID measurements, results in signals, whose integration leads to a very small (<1%) spin concentration. The simulated EPR parameters are listed in Table 3. Thus, electrochemical reductions of complex **1** can be summarized as follows:

$$[Cu^{II}_4(L^{\bullet})_4]^0 \overset{+e^-}{\underset{-e^-}{\rightleftharpoons}} [Cu^{II}_4(L^{\bullet})_3(L)]^1- \overset{+e^-}{\underset{-e^-}{\rightleftharpoons}} [Cu^{II}_4(L^{\bullet})_2(L)_2]^{2-} \overset{+e^-}{\underset{-e^-}{\rightleftharpoons}} [Cu^{II}_4(L^{\bullet})(L)_3]^{3-} \overset{+e^-}{\underset{-e^-}{\rightleftharpoons}} [Cu^{II}_4(L)_4]^{4-}$$

$[\mathbf{1}]^0$, $S_t = 0$ $\quad$ $[\mathbf{1}]^-$, $S_t = 1/2$ $\quad$ $[\mathbf{1}]^{2-}$, $S_t = 0$ $\quad$ $[\mathbf{1}]^{3-}$, $S_t = 1/2$ $\quad$ $[\mathbf{1}]^{4-}$, $S_t = 0$

$L^{\bullet}$ = iminosemiquinone(2-), L = amidophenolate (3-) (Chart I)

**Catalytic Oxidation of 2-Aminophenol.** We have examined the catalytic activity of complex **1** for the oxidation of 2-aminophenol by $O_2$ to 2-aminophenoxazine-3-one in methanol according to the reaction

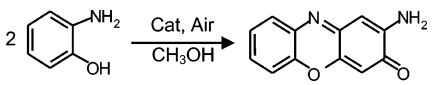


The reactivity studies were performed in methanol because of the good solubility of the complex as well as of the substrate and of its product. No base was added to the solutions to avoid the autoxidation of the substrate by air in the presence of a base. The above catalytic oxidation does not proceed in the absence of the catalyst, i.e., complex **1**.

Prior to a detailed kinetic study, we quantitatively evaluated the catalytic activity of the complex. For this purpose, $4.8 \times 10^{-6}$ mol of complex **1** in 20 mL of methanol was treated with 100 equiv of 2-aminophenol and stirred in air at ambient temperature for 40 h. The reaction was monitored spectrophotometrically at 435 nm ($\epsilon_{435} = 2.4 \times 10^4$ $M^{-1}$ $cm^{-1}$) to ensure its' completion. The product was analyzed by GC and GC-MS, which showed the formation of 2-aminophenoxazine-3-one by the aerial oxidation of 2-aminophenol as the sole product with 100% conversion.

The reaction kinetics were performed by observing the change in absorbance at 435 nm, which is characteristic of 2-aminophenoxazin-3-one in methanol. In a typical reaction, the catalyst was dissolved in methanol, the substrate, 2-aminophenol, was added, and the resulting light yellow-red solution was stirred in presence of air; the resultant spectral change as a function of time was measured. We have measured the kinetics of the oxidative catalysis under turnover conditions at 22 ± 1 °C using the initial rate method, where the concentration of the catalyst was varied in the range of $2.5 \times 10^{-5}$ to $2.5 \times 10^{-4}$ M and that of

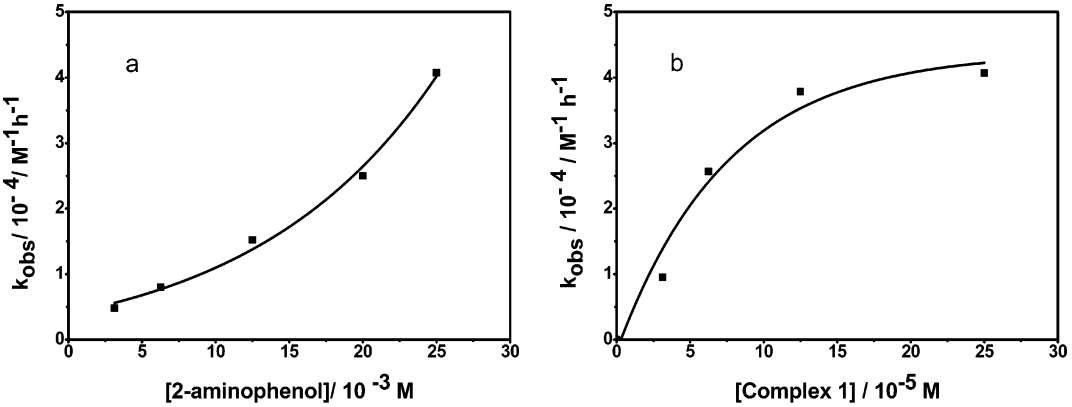


**Figure 9.** Variation of $k_{obs}$ with the concentrations of substrate and catalyst. (a) The line obtained from the fit to the equation $y = a + b_1x + b_2x^2$ with the fit parameters $a = 0.4485$, $b_1 = 0.0152$, $b_2 = 0.0051$ ($R^2 = 0.9938$). (b) The equation used for the fitting is $y = A \exp(-x/t) + y_0$, and the parameters are $y_0 = 4.386 \pm 0.524$, $A = -4.559 \pm 0.581$, and $t = 7.477 \pm 2.420$ M·h.

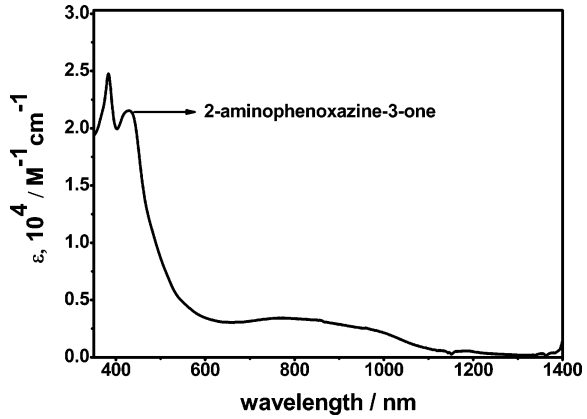


**Figure 10.** UV−vis/NIR spectrum of the reaction solution obtained from the glovebox.

2-aminophenol was in the range of $2.5 \times 10^{-3}$ to $2.5 \times 10^{-2}$ M. From the experimental rate constants depicted in Figure 9, an overall rate-law was deduced:

$$\text{rate} = k[\text{complex } \mathbf{1}][\text{2-aminophenol}]^2$$

The observed first-order dependence of the rate on the concentration of **1** and second-order dependence on 2-aminophenol indicate the composition of the activated complex; in other words, one molecule of complex **1** has been utilized for the six-electron oxidative coupling of two molecules of 2-aminophenol. The third-order rate law of the form rate = $k$[catalyst][substrate]$^2$ perhaps also suggests that a dimer of the substrate is rapidly formed from the monomeric substrate and that it is this dimer that reacts with the catalyst in the rate-determining step. The saturation kinetics in terms of the substrate (Figure 9b) indicate an equilibrium step involving both reaction partners via presumably hydrogen-bonding interactions through the OH group of the substrate.[8]

**Reaction under Anaerobic Conditions in a Glovebox.** To shed more light on this six-electron oxidation process, we performed additional experiments to demonstrate the following salient points: (i) The radicals coordinated to the Cu(II) centers are participating in the conversion process; (ii) oxygen of air is essential for the catalysis; and (iii) the stoichiometry and fate of oxygen involved.

Portions of 1 equiv of the tetranuclear complex **1** and 10 equiv of the substrate 2-aminophenol in $CH_3OH/CH_2Cl_2$ (1:4) solvent mixture were allowed to react for 40 h under argon in a glovebox.

An aliquot of this reaction solution was divided into two parts to (i) determine spectrophotometrically strictly under argon the amount of 2-aminophenoxazine-3-one formed in absence of air and to (ii) measure the concentration of hydrogen peroxide, extracted into an aqueous phase from the reaction solution by the titanyl sulfate reagent.

From the quantitative UV−vis spectral study (Figure 10) also strictly under argon, the formation of only 1 equiv of phenoxazinone chromophore could be observed, indicating that six electrons of **1** are involved. The concentration ratio [complex **1**]/[2-aminophenoxazin-3-one] evaluated after the reaction in the glovebox was found to be ∼1, strongly indicating that two molecules of 2-aminophenol react with one molecule of complex **1** to form one molecule of phenoxazinone chromophore. The process can then be summarized as

$$[Cu^{II}{}_4(L^{\bullet})_4]^0 + 2o\text{-aminophenol}$$

$$\text{glovebox} \downarrow CH_3OH/CH_2Cl_2\ (1{:}4)$$

$$[Cu^{II}{}_2Cu^{I}{}_2(L)_4]^{6-} + \text{2-aminophenoxazine-3-one}$$

It has been shown by electrochemistry that the first four reduction processes are ligand centered, which occur before the metal-centered reductions. Hence, for the above oxidative coupling under argon, reductions of four radical centers together with the reduction of two copper(II) centers are conceivable. This is also substantiated by comparing the UV−vis spectrum (Figure 10) of the reaction solution in the glovebox with that of the species[**1**]$^{4-}$, obtained from the four-electron electrochemical reduction of complex **1** (Figure 7); they are different. The broad band around 775 nm (Figure 10) with an absorption coefficient of 3400 $M^{-1}$ $cm^{-1}$ can be considered as an intervalence Cu(II)−Cu(I) band, as has been reported in the literature.[16]

The remaining reaction solution containing **1** from the glovebox was subjected to a quantitative absorption spectral

(16) Farrar, J. A.; Lappalainen, P.; Zumpft, W. G.; Saraste, M.; Thomson, A. J. *Eur. J. Biochem.* **1995**, *232*, 294.

**Scheme 2** Tentative Mechanism for the Formation of Phenoxazinone Chromophore[a]

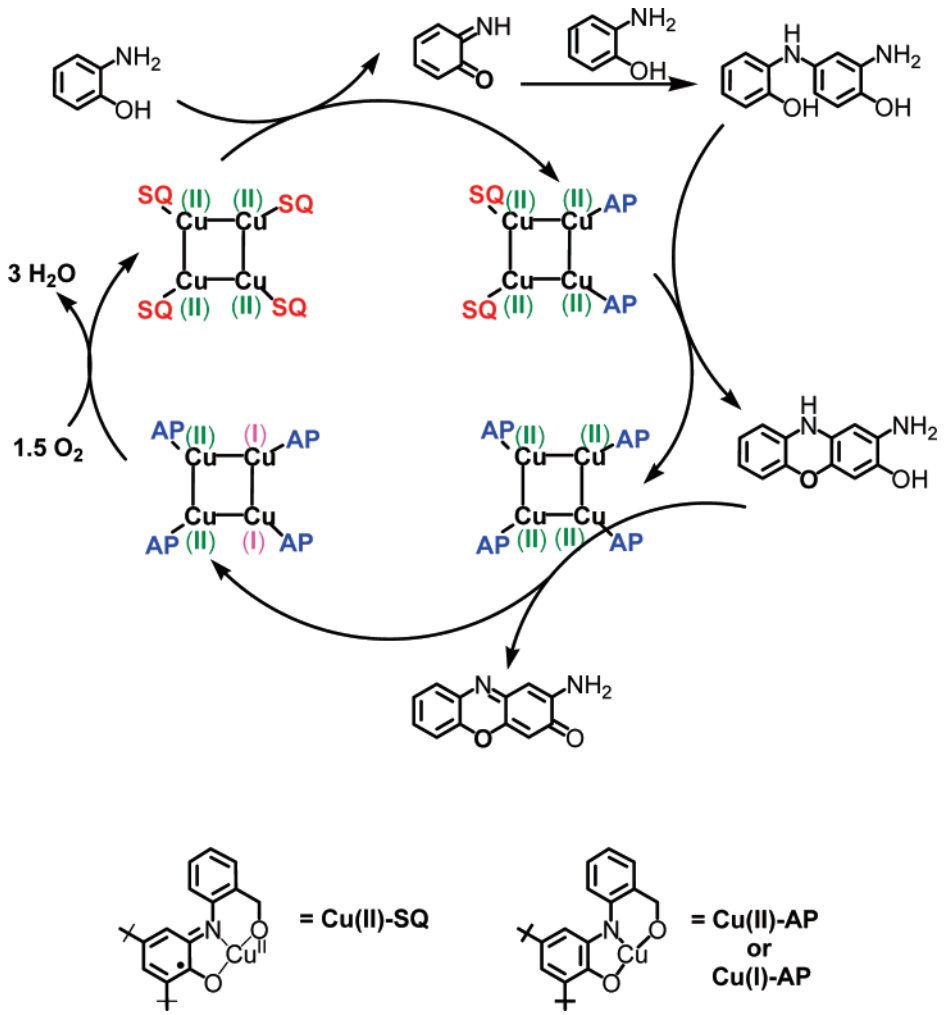


[a] The $Cu_4O_4$−cubane core has been represented by a rectangular tetracopper box for clarity.

study after long exposure to air to ascertain that 5 equiv of 2-aminophenoxazine-3-one had formed, indicating the essentiality of aerial oxygen for the catalytic process.

The presence of hydrogen peroxide in the catalytic solution could not be detected either by titanyl(IV)−sulfate reagent or by the liberation of iodine from an acidic potassium iodide solution, due to the catalase activity of the copper complex **1**. Moreover, due to the sluggish nature, the reaction at lower temperatures, for example, at −25 °C, it was not possible to detect or determine $H_2O_2$ (concentration), which decomposes at a much faster rate. Extremely slow nature of the oxidative coupling also prevented us from performing the $O_2$-uptake measurements accurately.

On the basis of the kinetic and electrochemical data and the anaerobic experiments described earlier, it is tempting to propose a mechanism involving stepwise pathways, keeping in mind that it is impossible to prove any single mechanism. A tentative catalytic cycle for the formation of the phenoxazinone chromophore is shown in Scheme 2.

It is clear that there is a complex interplay between the structural and electronic properties of the catalyst, **1**, in determining the hydrogen-bond formation,[8] which is essential for each encounter between the catalyst and the substrate leading to the oxidative process. The proton transfer followed by the electron transfer as implied in the mechanism (Scheme 2) may occur also as a hydrogen-atom transfer. Regeneration of the catalyst invokes participation of $O_2$, presumably resulting in the formation of an intermediate peroxo species involving the fully reduced form of the ligand AP, the amidophenolate anion, and copper(I). Such a peroxo species formed by $O_2$ binding to a very similar amidophenolate−antimony(V) center has been reported recently.[17]

A mechanism based on the radical intermediate, 2-aminophenoxyl, has been invoked in the literature for the similar oxidation of 2-aminophenol to the phenoxazinone chromophore using different copper salts under drastic conditions.[18] A few other complexes with cobalt and iron as PHS models are known in the literature to catalyze the oxidative coupling through a H-atom abstraction mechanism.[19] However, our proposed "off−on mechanism of the radicals" seems to be very common for the catalysis involving such metal−radical complexes.[7,8]

(17) Cherkasov, V. K.; Abakumov, G. A.; Grunova, E. V.; Poddelsky, A. I.; Fukin, G. K.; Baranov, E. V.; Kurskii, Y. V.; Abakumova, L. G. *Chem.—Eur. J.* **2006**, *12*, 3916.
(18) (a) Kaizer, J.; Csonka, R.; Speier, G. *J. Mol. Catal. A: Chem.* **2002**, *180*, 91. (b) Horváth, T.; Kaizer, J.; Speier, G. *J. Mol. Catal. A: Chem.* **2004**, *215*, 9.

## Conclusions and Outlook

As an obvious progression of our earlier reports,[6−10] an alkoxo-bridged tetranuclear copper(II)−iminosemiquinone complex containing as many as four radicals can be rationally synthesized. Antiferromagnetic exchange interactions of moderate strength have been evaluated from the variable-temperature magnetic susceptibility measurements (2−290 K) between the alkoxo-bridged Cu(II) centers and for the Cu(II)−radical interactions. A one *J* model has been found to efficiently describe the exchange interactions in the $Cu_4O_4$−cubane core of complex **1**.

The observations that we have made in the foregoing discussion indicate that complex **1** retains its solid-state structure with the cuboidal core in solution. Electrochemical measurements indicate redox processes that are ligand centered. Thus, for complex **1** four reversible reductions, resulting in the phenolate forms of the ligands, are discernible.

The investigation emphasizes that the tetracopper(II)-tetraradical complex **1** can catalyze the oxidation of 2-aminophenol with aerial oxygen as the sole oxidant to afford 2-aminophenoxazine-3-one in 100% yield under mild conditions to mimic the function of the copper-containing oxidase phenoxazinone synthase (PHS).

$$2(\text{2-aminophenol}) \xrightarrow[\text{air}]{\mathbf{1}\text{ in } CH_3OH} \text{2-aminophenoxazine-3-one}$$

An off−on mechanism of the radicals has been proposed for the catalytic process, in which three two-electron redox processes are operative. We have shown in previous works[8] the importance of hydrogen-bond formation for such catalysis. Thus, Mn(IV)−radical complexes have been found to catalyze the reactions of copper-containing enzymes like catechol oxidase and PHS.[7]

The ligand we have described here could also be applied to other transition metals, nickel(II), for example, which would allow for a variety of catalysis and spin coupling possibilities, thus suggesting a future direction of producing new bioinspired catalysts based on these metal−radical motifs.

**Acknowledgment.** Financial support from the Max-Planck Society and German Research Council (Deutsche Forschungsgemeinschaft) is gratefully acknowledged (project: Priority Program "Radicals in Enzymatic Catalysis" SPP 1071: Ch111/2-3).

IC7012599

(19) (a) Simándi, L. I.; Barna, T.; Németh, S. *J. Chem. Soc., Dalton Trans.* **1996**, 473. (b) Simándi, L. I.; Simándi, T. M.; May, Z.; Besenyei, G. *Coord. Chem. Rev.* **2003**, *245*, 85. (c) Simándi, T. M.; May, Z.; Szigyártó, I. C.; Simándi, L. I. *Dalton Trans.* **2005**, 365. (d) Simándi, T. M.; Simándi, L. I.; Gyór, M.; Rockenbauer, A.; Gömöry, A. *Dalton Trans.* **2004**, 1056.